VI

# CIGR HANDBOOK OF AGRICULTURAL ENGINEERING

## Information Technology

Edited by:
CIGR – The International Commission of Agricultural Engineering

Published by:
American Society of Agricultural and Biological Engineers

# CIGR Handbook of Agricultural Engineering

## Volume VI
## Information Technology

**Edited by CIGR – The International Commission of Agricultural Engineering**

**Volume Editor:**
**Axel Munack**
*Federal Agricultural Research Center, Braunschweig, Germany*

**Published by the**
**American Society of Agricultural and Biological Engineers**

58. Inoue, Y., B. A. Kimball, R. D. Jackson, P. J. Pinter Jr., and R. J. Reginato. 1990. Remote estimation of leaf transpiration rate and stomatal resistance based on infrared thermometry. *Agr. Forest Meteorol.* 51: 21-33.
59. Omasa, K., Y. Hashimoto, and I. Aiga. 1981. A quantitative analysis of the relationships between $SO_2$ or $NO_2$ sorption and their acute effects on plant leaves using image instrumentation. *Environ. Control Biol.* 19: 59-67.
60. Omasa, K., Y. Hashimoto, and I. Aiga. 1981. A quantitative analysis of the relationships between $O_3$ sorption and its acute effects on plant leaves using image instrumentation. *Environ. Control Biol.* 19: 85-92.
61. Omasa, K., and R. Funada. 1996. Image instrumentation of living plants. *BioSci. and Industry* 54: 545-546, 569-571.
62. Onoe, M., J. W. Tsao, H. Yamada, H. Nakamura, J. Kogure, H. Kawamura, and M. Yoshimatsu. 1983. Computed tomography for measuring annual rings of a live tree. *Proc. IEEE* 71: 907-908.

## 5.2 Remote Sensing from Satellites and Aircraft

*K. Omasa, K. Oki, and T. Suhama*

***Abstract.*** *This section introduces useful sensors for remote sensing from satellites and aircrafts using hyperspectral, hyperspatial, active, and 3-D observations. We also introduce recent advances in agricultural remote sensing including applications in sustainable agriculture such as precision farming, agroforestry, and land conservation.*

***Keywords.*** *Hyperspectral sensor, Land conservation, Land use, Lidar, Precision farming, Remote sensing.*

### 5.2.1 Introduction

Remote sensing from satellites and aircraft has been widely used for applications in agriculture [1-3]. In particular, passive optical sensors mounted on aircraft, Landsat, and SPOT (the French Systeme Probatoire d'Observation de la Terra) have allowed applications such as prediction of crop production and land use change. Recent advances in agricultural remote sensing are applications in sustainable agriculture, such as precision farming, agroforestry, and land conservation. These closely relate to applications in forest, ecosystem, hydrology, and environmental management [3-5].

Meanwhile, technical trends in remote sensing from satellites and aircraft are hyperspectral, hyperspatial, active, and 3-D observations [5-11]. Although ordinary satellite optical sensors, such as the Landsat Thematic Mapper (TM) and SPOT High Resolution Visible (HRV), have been limited to less than ten spectral channels, the Hyperion on Earth Observing-1 (EO-1) launched by NASAin November 2000 provides a high resolution hyperspectral imager capable of resolving 220 spectral bands (from 0.4 to 2.5 μm) with a 30-m spatial resolution. A hyperspatial QuickBird satellite launched in October 2001 provides panchromatic (PAN) images with a spatial resolution of

about 0.6 m. The use of active remote sensors such as lidar and SAR can provide more useful information than can passive sensors. For example, the Vegetation Canopy Lidar (VCL), which will be launched in the near future, will be able to measure 3-D ground surface and vegetation canopy with 1-m elevation accuracy by Nd:YAG diode-pumped pulse lasers of a 25-m footprint [12]. Recent advances in aircraft remote sensing are similar to those in satellite remote sensing. Hierarchical remote sensing, which joins image sensing described in Section 5.1 with remote sensing from satellites and aircraft, may be submitted for more effective use in sustainable agriculture.

In this section, therefore, useful remote sensing sensors mounted on satellites and aircraft, and several applications in agriculture, are described.

### 5.2.2 Sensors for Remote Sensing

The major kinds of information obtained by remote sensing from satellites and aircraft is summarized in Table 1.

#### *Remote Sensors on Satellites*

*MSS, TM and ETM+ (Landsat, NASA, USA)*

The *Multispectral Scanner (MSS)* is an optical sensor mounted on Landsat 1 to Landsat 5. Landsat 1, with the MSS, was launched in 1972 and has verified the effectiveness of remote sensing from space. The MSS has four bands in the visible to the near-infrared region: 0.5 to 0.6 μm (band 4), 0.6 to 0.7 μm (band 5), 0.7 to 0.8 μm (band 6), and 0.8 to 1.1 μm (band 7). The spatial resolution is approximately 80 m. Furthermore, the MSS mounted on Landsat 3 is equipped with a thermal infrared band (10.4 to 12.5 μm) with a spatial resolution of 240 m.

The *Thematic Mapper (TM)* is an optical sensor mounted on Landsat 4 and Landsat 5. It has seven bands, which are 0.45 to 0.52 μm (band 1), 0.52 to 0.60 μm (band 2), 0.63 to 0.69 μm (band 3), 0.76 to 0.90 μm (band 4), 1.55 to 1.75 μm (band 5), 10.40 to

**Table 1. Major information obtained by remote sensing.**

| |
|---|
| Multi- or hyperspectral remote sensing (visible region to near-infrared region) |
| • Land (farmland, forests, natural vegetation, etc.):<br>Terrain, land cover, land use, vegetation indices, plant species, phenology, biomass, crop yield, visible injuries, canopy biochemistry, soil types, chemical and physical properties of soils, fertilizer application, water status, snow and ice, water resources |
| • Hydrosphere (does not include atmosphere):<br>Coral shelves, terrain of shallows, water pollution, plankton |
| • Atmosphere:<br>Clouds, water vapor, fog, aerosols, dust, air pollution |
| Thermal remote sensors |
| Thermal radiation, temperature of land and water area, evapotranspiration (including transpiration of plants), soil moisture, atmospheric temperature, ocean currents, clouds |
| Lidar |
| Terrain, 3-D canopy structure, biomass, aerosols, air pollutants, advective diffusion |
| SAR |
| Terrain, surface structure, clouds, rainfall |

12.50 μm (band 6), and 2.08 to 2.35 μm (band 7). The spatial resolution of these bands, except band 6 (120 m), is 30 m. In comparison with the MSS, the TM is improved regarding the increased number of spectral bands and spatial resolution. As a result, the accuracy of land cover classification has been improved. Furthermore, by using these new wavelength ranges, such as band 3 and band 4, various vegetation indices for estimating vegetation conditions have been developed.

The *Enhanced Thematic Mapper Plus (ETM+)* is a sensor mounted on Landsat 7, launched in 1999. It is an improved version of the TM sensor on Landsat 4 and 5. The advantage of ETM+ is the improvement in spatial resolution of the thermal infrared band (band 6, spatial resolution of 60 m) and the addition of the panchromatic band (0.50 to 0.90 μm, 15 m). In the future, applications using the thermal infrared band will become popular in the field of agriculture.

*Hyperion (EO-1, NASA, USA)*

The *Hyperion,* mounted on Earth Observing-1 (EO-1) launched in 2000, is a high resolution hyperspectral imager capable of resolving 220 spectral bands (0.4 to 2.5 μm) with a 30-m spatial resolution. It is collecting hyperspectral scenes over the course of its mission in coordination with the ETM+ on Landsat 7. Both Hyperion and ETM+ survey the same ground areas. Detailed comparisons of the Hyperion and ETM+ images may expand future applications in agriculture, forest, mining, geology, and environmental management.

*ASTER (EOS AM-1, NASA, USA)*

The *Advanced Spaceborne Thermal Emission and Reflection Radiometer (ASTER)* is an optical sensor mounted on EOS AM-1 launched in 1999. The ASTER has 3 bands (0.52 to 0.86 μm) with a spatial resolution of 15 m, 6 bands (1.60 to 2.43 μm) with a spatial resolution of 30 m, and 5 bands (8.125 to 11.65 μm) with a spatial resolution of 90 m. The ASTER is expected to be useful in various fields such as underground resourcing, environmental monitoring, and volcanic activity monitoring.

*HRV and HRVIR (SPOT, CNES, France)*

The *High Resolution Visible (HRV)* is an optical sensor mounted on SPOT 1, 2, and 3, and the *High Resolution Visible Infrared (HRVIR)* is mounted on SPOT 4. The SPOT was designed by the Centre National d'Etudes Spatiales (CNES), France. SPOT 1 was launched in 1986, SPOT 2 in 1990, SPOT 3 in 1993, and SPOT 4 in 1998. The HRV on SPOT 1 to 3 has two modes, namely multispectral and panchromatic modes. In the multispectral mode, there are three bands of 0.50 to 0.59 μm (band 1), 0.61 to 0.68 μm (band 2), and 0.79 to 0.89 μm (band 3) with the spatial resolution of 20 m. In the PAN mode, the spatial resolution is 10 m of 0.51 to 0.73 μm wavelength. The modifications from HRV to HRVIR on SPOT 4 are the improvement in spatial resolution of band 2 (10 m) and the addition of short-wave infrared band from 1.58 to 1.75 μm (band 4, 20 m). The remotely sensed imagery measured by these sensors provides vegetation maps, lithologic maps, and detailed ground surface information. Furthermore, SPOT 5 was launched in 2002. It was improved to a spatial resolution of 10 m in band 1 to band 3 and of 2.5 m and 5 m in the PAN band from 0.48 to 0.71 μm.

*IKONOS (Space Imaging, USA)*

The *IKONOS* is an earth-observation satellite launched by Space Imaging/EOSAT in 1999. The major advantage of IKONOS is its high spatial resolution. For example, the spatial resolution of PAN (0.45 to 0.90 μm) and multispectral [0.45 to 0.52 μm (blue), 0.52 to 0.60 μm (green), 0.63 to 0.69 μm (red), and 0.76 to 0.90 μm (Near-IR)] bands is 0.82 m and 3.3 m, respectively. The high spatial resolution images measured by IKONOS are used for applications in urban, forest, and agricultural areas like airborne remote sensing images. These are also expected to be useful in precision farming.

*QuickBird (DigitalGlobe, USA)*

The *QuickBird* of DigitalGlobe was launched in 2001. The spectral bands of QuickBird are similar to those of IKONOS. However, QuickBird has higher spatial resolution. The spatial resolution of PAN (0.45 to 0.90 μm) and multispectral [0.45 to 0.52 μm (blue), 0.52 to 0.60 μm (green), 0.63 to 0.69 μm (red), and 0.76 to 0.90 μm (Near-IR)] bands are 0.61 m and 2.44 m, respectively. The QuickBird is expected to have effective use in urban, forest, and agriculture applications, like the IKONOS.

*AVHRR (TIROS-T and NOAA, NOAA, USA)*

Initially the *Advanced Very High Resolution Radiometer (AVHRR)* was mounted on TIROS-N, launched in 1978, and later the AVHRR was also mounted on NOAA. The basic specifications of AVHRR have not changed, and the AVHRR has been continually utilized for earth observation. The current AVHRR has five bands, which are 0.58 to 0.68 μm (band 1), 0.725 to 1.1 μm (band 2), 3.55 to 3.93 μm (band 3), 10.3 to 11.3 μm (band 4), and 11.5 to 12.5 μm (band 5). The AVHRR provides spatial resolution of approximately 1.1 km and a swath 2399 km wide. As NOAA orbits the globe 14 times daily, the AVHRR observes the same area twice a day. The wide-swath images measured by AVHRR are useful for various purposes, for example, for obtaining changes in cloud cover and land cover, vegetation index, and surface temperature. Consequently, these provide valuable information on surface properties and weather over regional scales.

*MODIS (EOS AM-1 and PM-1, NASA, USA)*

The *Moderate Resolution Imaging Spectroradiometer (MODIS)* is an optical sensor mounted on EOS AM-1 and PM-1, launched in 1999 and 2002, respectively. The MODIS has 21 bands (0.4 to 3.0 μm) and 15 bands (3.0 to 14.5 μm). The spatial resolutions are 250 m (2 bands), 500 m (5 bands), and 1,000 m (29 bands). The MODIS can observe any site on the earth surface every 2 days. In the future, the wide-swath image measured by MODIS will be used effectively for earth observation like the AVHRR.

*SAR (JERS-1, Japan, ERS-1/2, EU, RADARSAT, Canada)*

The *Synthetic Aperture Radar (SAR)* is an active sensor, which is used to observe physical properties, roughness, and inclination of the ground level using microwaves. The observation is almost independent of weather conditions, and it can be done through clouds. In particular, applications in vegetation classification of forests, grasslands, and agriculture areas have been studied using L (15 to 30 cm), C (3.75 to 7.5

cm), and X (2.4 to 3.75 cm) bands mounted on JERS-1, ERS-1/2, and RADARSAT, respectively.

*Remote Sensors on Aircraft*

Aircraft remote sensing has the advantages of flexible use and high spatial resolution in comparison with satellite remote sensing. For example, although the Landsat captures images of a region every 16 days, only several images are useful within a year; aircraft remote sensing can provide more images that could be used in analysis of rapid changes of seasons. Therefore, for development of agricultural remote sensing, it is necessary to use both satellite and aircraft remote sensing.

*AVIRIS (JPL, NASA, USA)*

The *Airborne Visible Infrared Imaging Spectrometer (AVIRIS)* is a hyperspectral image sensor developed by the Jet Propulsion Laboratory (JPL). The AVIRIS covers the range of 0.4 to 2.5 μm in 224 contiguous bands approximately 10 nm wide and allows 20-m spatial resolution. The hyperspectral bands are expected for use in more exact classification of land cover and vegetation, diagnosis of crops, and identification of chemical compositions of soils.

*CASI (ITRES Research Ltd, Canada)*

The Compact Airborne Spectrographic Imager (CASI) is a hyperspectral sensor like the AVIRIS. Features of the CASI are a push-broom charge coupled device (CCD) with high spatial resolution (0.5 to 10 m) and an adjustable spectral range between 0.4 and 1.0 μm of up to 288 programmable spectral bands at 1.9 nm intervals.

*AISA (Spectral Imaging, USA)*

The *Airborne Imaging Spectroradiometer for Application (AISA)* is a hyperspectral sensor with a 2-m spatial resolution, developed by Spectral Imaging Ltd. The wavelength range is 0.43 to 1.0 μm and 512 spectral bands are the maximum. The AISA sensor head includes a fiber optic probe (FODIS) for real-time monitoring of downwelling solar irradiance to calculate the apparent reflectance of the earth's surface.

*ADS40 (LH Systems, USA)*

The *Airborne Digital Sensor (ADS40)* was developed by LH Systems and the German Aerospace Center. It has forward-, nadir-, and backward-looking linear CCD arrays to provide high spatial-resolution panchromatic images. The three line stereo images are captured simultaneously, and the triple overlap of the images provides high-quality DTM (digital terrain model). The ADS40 has further arrays for multispectral data (blue, B: 0.43 to 0.49 μm, green, G: 0.535 to 0.585 μm, red, R: 0.61 to 0.66 μm and near-infrared, NIR: 0.835 to 0.885 μm). The multispectral data can be used for applications in crop and land use analysis with a high spatial resolution of 20 cm.

*ALTM (Optech, Canada)*

The *Airborne Laser Terrain Mapper (ALTM)* is a series of airborne lidars (light detection and ranging), manufactured by Optech, for 3-D range measurement and terrain mapping. The ALTM 1025 has a scanning range finder with a range resolution of 1 cm and a range accuracy within 15 cm. The wavelength and beam divergence of the used laser (Nd:YAG) are 1,064 nm and 1.2 mrad (or 0.25 mrad). The frequencies of

pulse repetition and scan are 25,000 Hz and 25 Hz, respectively. The sampling data per one scan are 1,000 points. This system is expected to be useful in estimating the 3-D structure of woody canopies and vegetation biomass as well as terrain mapping.

In addition to those mentioned above, numerous remote sensors for aircraft, such as multi- and hyperspectral optical imagers, lidars, SARs, are produced by government agencies and private companies. The images measured by aircraft remote sensors require complicated rectification of aircraft tilt, shift, and flying height. Data of aircraft geometry from on-board GPS and *Inertial Measurement Units* (GPS/IMU) are used to rectify aircraft sensor images precisely.

### 5.2.3 Analysis of Land Use and Nitrogen Flow Using Data of Landsat and GIS

#### *Classification of Land Use with LANDSAT MSS*

The eutrophication of lakes and rivers is closely related with increases in population and industrial and agricultural activities [13,14]. Therefore, relationships between eutrophication and land use change have been analyzed using Landsat and GIS data.

Figure 1 shows the basins of rivers flowing into two lakes and changes in land use in the basins from 1979 to 1990 [15]. The lakes lie 60 to 90 km northeast of Tokyo. Lake Kasumigaura is the second largest lake in Japan with a water area of 220 $km^2$ and a basin area of 2,135 $km^2$. The water depth is shallow, ranging from 0 to 7 m with an average of 4 m. In the lake, eutrophication is caused by influent nutrients such as nitrogen and phosphorous from the basins, and consequently algal blooms grow during the summer. As shown in Figure 1, the basin of each river was isolated using DEM (digital elevation model). The land cover was classified into five categories (urban area, paddy field, forest area, other crop land, and water area) using LANDSAT MSS data observed in 1979, 1984, and 1990. The urban area has rapidly increased along roads around railway stations and big cities, and consequently other areas have decreased.

#### *Analysis of Nitrogen Flow from Different Land Use Areas to Lakes*

The inflow of nitrogen from the basin to the lake is a major factor in eutrophication. Therefore, the nitrogen flow from different land use area to the lake is analyzed by the following.

Annual nitrogen flow ($L_i$, kg/y) from a basin area ($i$) of one river to the lake is given by:

$$L_i = 10^{-3} C_i \cdot Q_i \tag{1}$$

where $C_i$ (mg/l) is the annual mean value of total nitrogen concentration in the river near the mouth, and $Q_i$ ($m^3$/y) is the annual water flow of the river.

A ratio of $L_i$ to the total area ($A_i$, $km^2$) of the basin $i$ is expressed by:

$$\frac{L_i}{A_i} = \sum_{j=1}^{4} (U_j \cdot r_{ij}) \tag{2}$$

where $j$ (= 1 to 4) is for each category of urban area, paddy field, forest area, or other crop land; $U_j$ (kg·km$^{-2}$·y$^{-1}$) is the coefficient called the runoff load factor of each category $j$; and $r_{ij}$ is the ratio of area ($A_{ij}$, km$^2$) of each category $j$ to $A_i$ in the basin $i$.

The $C_i$ was calculated from data measured at ten large rivers. $Q_i$ was estimated from annual precipitation and run-off ratios of each river basin. $A_i$ and $r_{ij}$ were calculated from results in Figure 1. Because $U_j$ for only four categories are unknown, these were estimated by minimizing $E$ in the following equation.

$$E = \sum_i \left( \frac{L_i}{A_i} - \sum_{j=1}^{4} (U_j \cdot r_{ij}) \right)^2$$

Figure 2 shows estimated runoff load factors ($U_j$) of total nitrogen for four categories. The runoff load factors for forest area and paddy field were almost zero. However, those for the urban area and other crop land showed large values. The decrease in

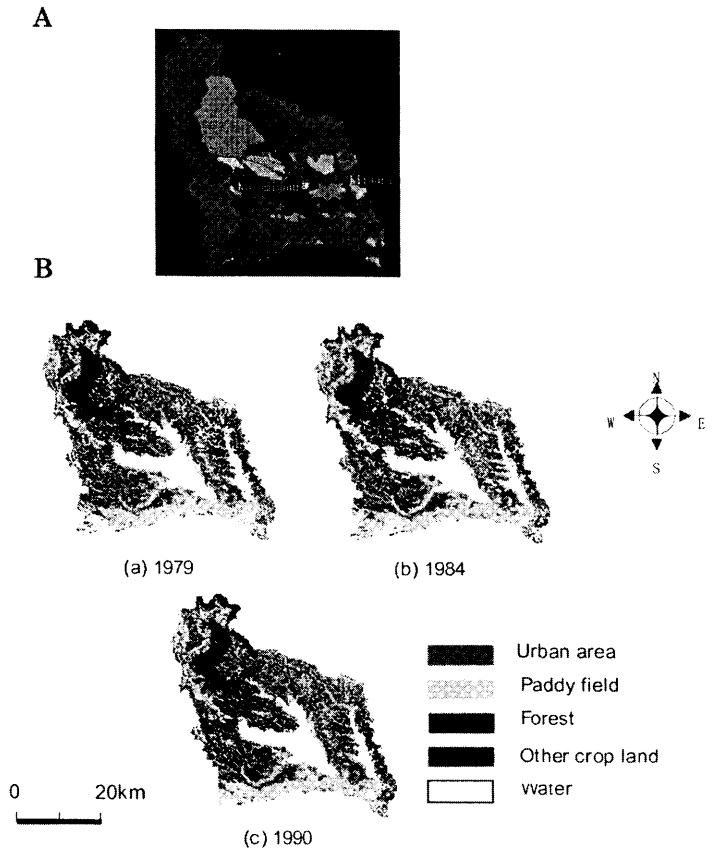


**Figure 1. Basins of rivers flowing into lakes Kasumigaura and Kitaura in Japan (A) and changes in land use in the basins (B). Each area in (A) represents the isolated basin of each river [15].**

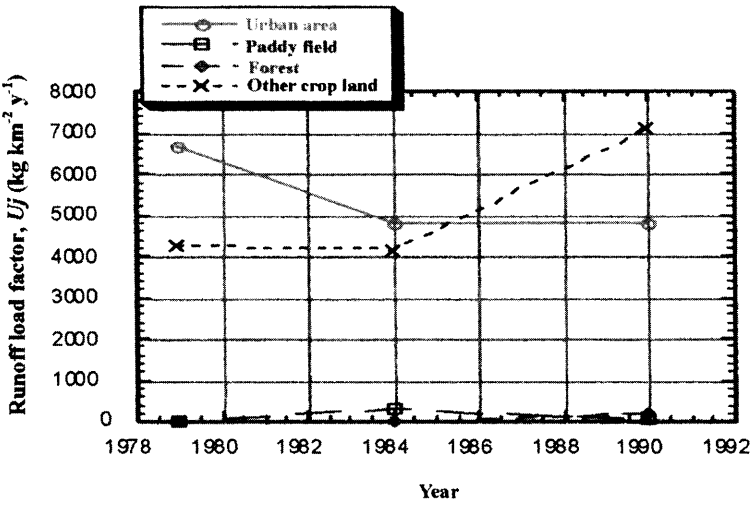


**Figure 2. Differences in runoff load factor of total nitrogen among urban areas, paddy fields, forests, and other crop fields [15].**

urban area runoff from 1979 to 1984 may be due to the spread of sewers. The increase in other crop field runoff from 1984 to 1990 may be caused by expansion of pig farming. The difference in precipitation may also have an affect on the runoff load. It is concluded that the extension of urban areas and crops fields other than paddy fields increases the eutrophication of Lake Kasumigaura through the rise of nitrogen flow to the lake.

### 5.2.4 Estimation of Wheat Growth Using Aerial Hyperspatial Data

Oversupply of fertilizers and agrichemicals in agriculture causes pollution of soil and water. Precision farming is a concept for increasing plant production and optimizing use of water, fertilizers, and agrichemicals [16-18]. The spatial distributions of these materials in farmland are not uniform. Therefore, hierarchical remote sensing, which joins image sensing (described in Section 5.1) with remote sensing, is expected to be one of the important tools for precision farming.

Figure 3 shows a *normalized differential vegetation index (NDVI)* image calculated from aerial hyperspatial images measured by the above-mentioned ADS40 (LH Systems, USA). The wheat field is the same place as that shown in Figure 3 of Section 5.1. In each test area ($8 \times 8$ m$^2$) of the field, nitrogen fertilizer at 0.0, 0.1, or 0.2 kg/m$^2$ was applied before seeding in the previous year. The multispectral images of four bands (R, G, B and NIR) with a spatial resolution of about 20 cm were measured in the following spring during the growing period of wheat crops. The NDVI was calculated using R (0.610 to 0.660 μm) and NIR (0.835 to 0. 885 μm) images by the following equation:

$$NDVI = \frac{NIR - R}{NIR + R} \tag{3}$$

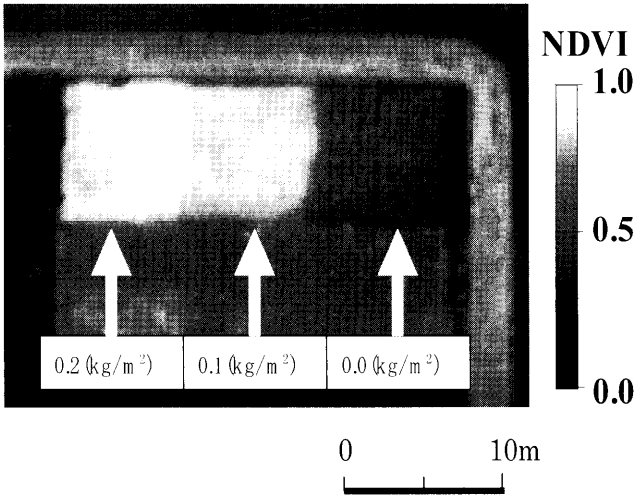


**Figure 3. NDVI image of wheat field with applications of different amounts of nitrogen fertilizer.**

The NDVI is a multipurpose index of contents of plant pigments, especially chlorophyll *a*, relating to photosynthesis, net primary production (NPP), and leaf area index (LAI) [1,19-26]. It ranges between –1 and 1. The increase of chlorophyll *a*, NPP, and LAI during the adult phase before the reproductive phase lowers red-light reflectance against high near-infrared reflectance, and consequently, the NDVI increases.

As shown in Figure 3, two test areas with the fertilizer application had high growth rates and high values of NDVI. However, the value of the right area without the fertilizer application was as low as that of grass area under the test area. The soil area of the left side and the asphalt road of the upper and right borders showed lower values than other areas. The road edge between the test area and the asphalt road showed values between the grass area and the test area with high growth rate. Although wheat crops of the middle area grew normally, those of the left area with the highest value of NDVI had a low tolerance to wind. This result suggests noteworthy points in use of NDVI.

### 5.2.5 Analysis of Farmland Using Aerial Hyperspectral Data

Hyperspectral data are useful for analyzing spectral properties of various crops and other land covers such as soils in farmland [27-31]. Figure 4 shows spectral properties of four areas covered by three crops (watermelon, maize, and taro) and loamy soil in farmland in the Miura Peninsula, about 50 km south of Tokyo. The spectral properties were obtained from aerial hyperspectral images, of 70 bands in a range of 0.43 to 0.90 μm and 2 m spatial resolution, measured by the AISA (Spectral Imaging, USA). The Miura Peninsula is a typical area of suburban agriculture in Japan. In the farmland, which is divided into small fields, many vegetable crops such as watermelon, maize, taro, cabbage, pumpkin, and Japanese radish are cultured year-around because of warm weather conditions.

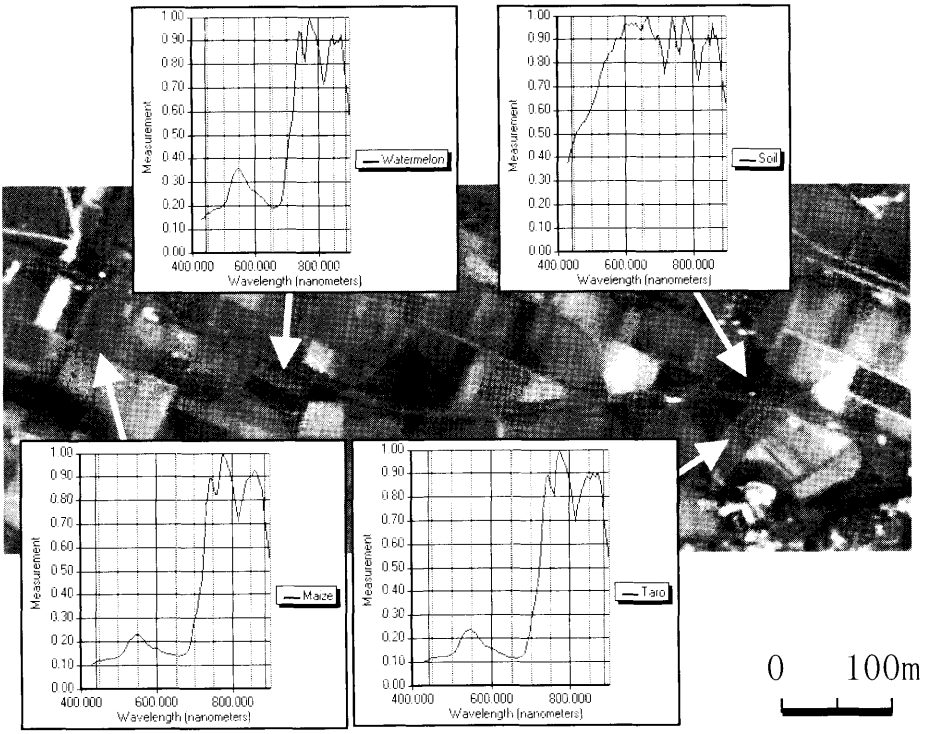


**Figure 4. Spectral properties of three crop fields (watermelon, maize, and taro plants) and loamy soil in farmland, obtained from aerial hyperspectral images.**

In Figure 4, the spectral properties of crops represent large absorptions caused by photosynthetic pigments in the visible range: a steep increase in the red-edge region from 0.69 to 0.74 μm continuing high to 0.9 μm, similar to the leaf reflectance spectra shown in Figure 1 of Section 5.1. The properties of loamy soil also are similar to those in Figure 1 and these are clearly different from those of vegetable crops. However, there are several drops in the high reflectance region beyond 0.74 μm. These are caused by $O_2$ (at 0.76 μm) in the atmosphere; by $H_20$ (at 0.96 μm) in the atmosphere, crops and soils; and by other factors. The analysis of spectral properties in the visible to near-infrared region may provide more useful information on contents of pigments, water, minerals, and nutrients, as well as crop species, production, and growth conditions. Therefore, hyperspectral remote sensing is expected to be a key tool for precision farming.

### 5.2.6 3-D Remote Sensing of Terrain and Forests Using Aerial Lidar Data

Aerial scanning lidar is an emerging *active* remote sensing technology for direct 3-D terrestrial observation [7,9-11]. Figure 5 shows 3-D images of terrain (ground surface) and a woody canopy obtained by a helicopter-borne scanning lidar (ALTM 1025

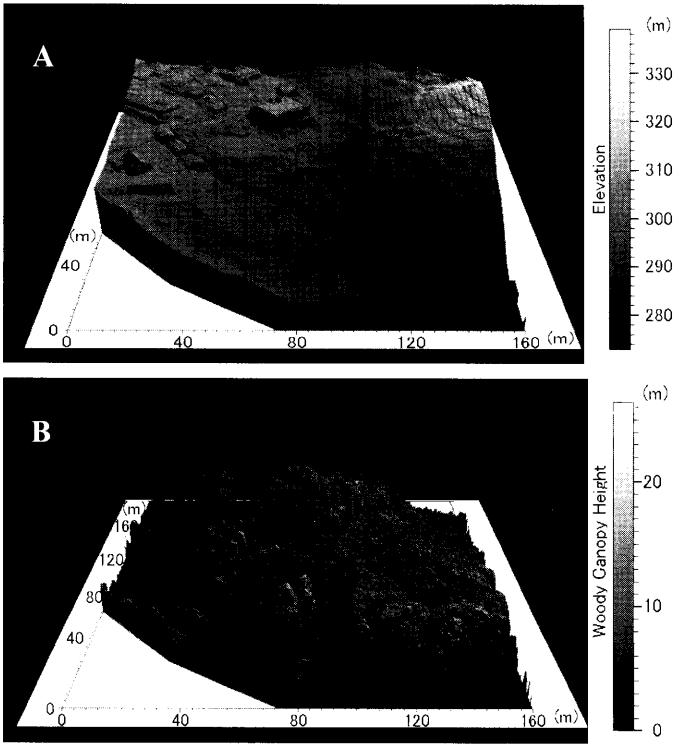


**Figure 5. 3-D images of terrain (A, ground surface) and woody canopy (B) obtained by a helicopter-borne scanning lidar with high spatial resolution [9].**

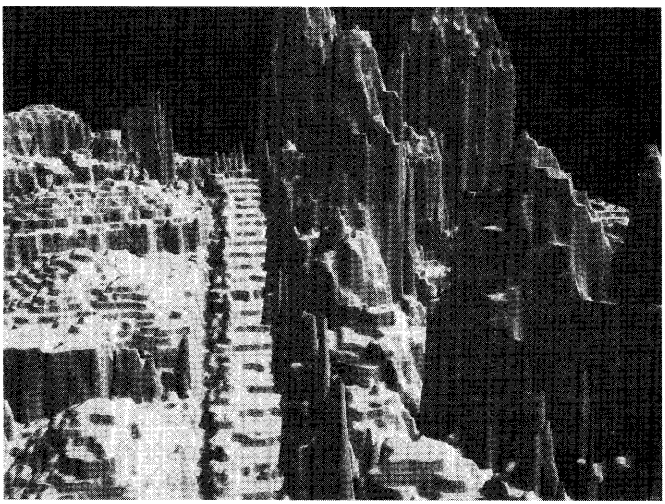

**Figure 6. 3-D close-up view of first pulse mode DEM of a place in Figure 5 [9].**

special model, Optech Co., Canada and Aero Asahi Co., Japan) with a high spatial resolution (about 33 cm mesh). The terrain of a valley was estimated with an accuracy of about 15 cm by interpolation of DEM data measured using a last-pulse mode, measuring the longest elapsed time between the emitted pulse of laser and the returned pulse. The woody canopy height was calculated by subtracting the terrain from DEM data measured using a first-pulse mode measuring the shortest elapsed time. The laser-derived tree heights were in error by less than 47 cm (RMSE = 19 cm) for coniferous trees and 40 cm (RMSE = 12 cm) for broadleaf trees.

Figure 6 shows a 3-D close-up view of first pulse mode DEM of a place in Figure 5. In left area of the place, the land is been turned into housing lots. There are several trees on the right. A straight narrow path with a flight of stairs is in the center. These stairs in the image were caused by digitization of the image (quantization error = about 15 cm).

We are studying farmland and public garden planning, forest management, carbon stock (biomass) estimation of forests by using this system and portable scanning lidars in addition to passive 2-D remote sensing data [9,11,32]. In the near future, these systems will be used effectively to assess forest development relating to forestation, agro-forestry, and water resource management.

## References


1. Myers, V. I. 1983. Remote sensing applications in agriculture. *Manual of Remote Sensing,* 2nd ed., Vol.III, ed. R. N. Colwell, 2111-2228. VA: Amer. Soc. Photogrammetry.
2. Steve, M. D., and J. A. Clark, eds. 1990. *Applications of Remote Sensing in Agriculture*. London, UK: Butterworths.
3. Owe, M., and G. D'Urso, eds. 2002. *Remote Sensing for Agriculture, Ecosystems, and Hydrology III*. Bellingham, WA: SPIE.
4. Hobbs, R. J., and H. A. Mooney, eds. 1990. *Remote Sensing of Biosphere Functioning*. New York, NY: Springer.
5. Rencz, A. N. 1999. *Remote Sensing for the Earth Sciences*. New York, NY: John Wiley and Sons.
6. Campbell, B. J. 1996. *Introduction to Remote Sensing*. New York, NY: The Gulford Press.
7. Flood, M., and B. Gutelious. 1997. Commercial implications of topographic terrain mapping using scanning airborne laser radar. *Photogramm. Eng. Remote Sens.* 63: 327-366.
8. Henderson, F. M., and A. J. Lewis, eds. 1998. *Principles and Applications of Imaging Radar*. New York, NY: John Wiley and Sons.
9. Omasa, K., Y. Akiyama, Y. Ishigami, and K. Yoshimi. 2000. 3-D remote sensing of woody canopy heights using a scanning helicopter-borne lidar system with high resolution. *J. Remote Sens. Soc. Jpn.* 20: 394-406.
10. Lefsky, M. A., W. B. Cohen, G. G. Parker, and D. J. Harding. 2002. Lidar remote sensing for ecosystem studies. *BioSci.* 52: 19-30.

11. Omasa, K., G. Y. Qiu, K. Watanuki, K. Yoshimi, and Y. Akiyama. 2003. Accurate estimation of forest carbon stocks by 3-D remote sensing of individual trees. *Environ. Sci and Tech.* 37: 1198-1201.
12. Dubayah, R., J. B. Blair, J. L. Bufton, D. B. Clark, J. Jaja, R. Knox, S. B. Luthcke, S. B. Prince, and J. Weishampel. 1997. The vegetation canopy lidar mission. *Proceedings of Land Satellite Information in the Next Decade, II: Sources and Applications*, 100-112. Bethesda, MD: Am. Soc. Photogramm. Eng. Remote Sens.
13. Krenkel, P. A., and V. Novotny 1980. *Water Quality Management.* London, UK: Academic Press.
14. Lewis Jr., W. M., J. F. Saunders III, D. W. Crumpacker Sr, and C. Brendecke. 1984. *Eutrophication and Land Use.* New York, NY: Springer-Verlag.
15. Oki, K., Y. Yasuoka, and M. Inamura. 1998. Estimation of annual total nitrogen load to lake from basin with remote sensing. *Proceedings the 19th Asian Conference on Remote Sensing, Philippines,* Q61-66. http://www.gisdevelopment .net/aars/acrs/1998/ps2/ps2006.shtml.
16. Hegg, R. 1999. Sustainable and environmental engineering. *CIGR Handbook of Agricultural Engineering,* Vol.III, eds. B. A. Stout, and B. Cheze, 585-598. St. Joseph, MI: ASAE.
17. Auernhammer, H., and J. K. Schueller. 1999. Precision farming. *CIGR Handbook of Agricultural Engineering,* Vol.III, eds. B. A. Stout and B. Cheze, 598-616. St. Joseph, MI: ASAE.
18. De Baerdemaeker, J., A. Munack, H. Ramon, and H. Speckmann. 2001. Mechatronic systems, communication, and control in precision agriculture. *IEEE Contr. Syst. Mag.* 21: 48-70.
19. Tucker, C. J. 1979. Red and photographic infrared linear combinations for monitoring vegetation. *Remote Sens. Environ.* 8: 127-150.
20. Jackson, R. D., P. N. Slater, and P. J. Pinter. 1983. Discrimination of growth and water stress in wheat by various vegetation indices through clear and turbid atmospheres. *Remote Sens. Environ.* 15: 187-208.
21. Hinzman, L. D., M. E. Bauer, and C. S. T. Daughtry. 1986. Effects of nitrogen fertilization on growth and reflectance characteristics of winter wheat. *Remote Sens. Environ.* 19: 47-61.
22. Tucker, C. J., W. W. Newcomb, S. O. Los, and S. D. Prince. 1991. Mean and inter-year variation of growing-season normalized difference vegetation index for the Sahel 1981-1989. *Int. J. Remote Sens.* 12: 1113-1115.
23. Fernandez, S., D. Vidal, and E. Simon. 1994. Radiometric characteristics of *Triticum aestivum* cv. Astral under water and nitrogen stress. *Int. J. Remote Sens.* 15: 1867-1884.
24. Reddy, G. S., C. L. N. Rao, L. Venkataratnam, and P. V. K. Rao. 2001. Influence of plant pigments on spectral reflectance of maize, groundnut and soybean grown in semi-arid environments. *Int. J. Remote Sens.* 22: 3373-3380.
25. Singh, R., D. P. Semwal, A. Rai, and R. S. Chhikara. 2002. Small area estimation of crop yield using remote sensing satellite data. *Int. J. Remote Sens.* 23: 49-56.

26. Silleos, N., K. Perakis, and G. Petsanis. 2002. Assessment of crop damage using space remote sensing and GIS. *Int. J. Remote Sens.* 23: 417-427.
27. Demetriades-Shah, T. H., M. D. Steven, and J. A. Clark. 1990. High resolution derivative spectra in remote sensing. *Remote Sens. Environ.* 33: 55-64.
28. Malthus, T. J., B. Andriew, F. M. Danson, K. W. Jaggard, and M. D. Steven. 1993. Candidate high spectral resolution infrared indices for crop cover. *Remote Sens. Environ.* 46: 204-212.
29. Carter, G. A. 1994. Ratios of leaf reflectances in narrow wavebands as indicators of plant stress. *Int. J. Remote Sens.* 15: 697-703.
30. Cochrane, M. A. 2000. Using vegetation reflectance variability for species level classification of hyperspectral data. *Int. J. Remote Sens.* 21: 1113-1115.
31. Kokaly, R. F. 2001. Investigating a physical basis for spectroscopic estimates of leaf nitrogen concentration. *Remote Sens. Environ.* 75: 153-161.
32. Omasa, K., Y. Urano, H. Oguma, and Y. Fujinuma. 2002. Mapping of tree position of *Larix leptolepis* woods and estimation of diameter at breast height (DBH) and biomass of the trees using range data measured by a portable scanning lidar. *J. Remote Sens. Soc, Jpn.* 22: 550-557.

## 5.3 Speaking Plant/Speaking Fruit Approaches

*Y. Hashimoto, T. Morimoto, and J. De Baerdemaeker*

***Abstract.*** *A skilled grower can deal well with various plants and yield good products using intuition and visual information, in those ways communicating with the plants. To optimize plant production scientifically, it is important to measure plants' physiological responses using sensors and then use that information for control. Such an approach is called the speaking plant approach (SPA), where environmental factors are the input variables and the plant responses are the output variables. The term* speaking plant (SP) *refers to plant responses that are measured using sensors. This approach is also applicable to storage processes and is called a speaking fruit approach (SFA). Measurement, identification, and optimization of plant (or fruit) responses, as affected by environmental factors, are important tasks for the SPA (or SFA). It is, however, difficult to sufficiently address these tasks because plant responses are quite complex and uncertain, but intelligent control techniques can facilitate such tasks. This section introduces SPA and SFA concepts and then presents an intelligent control technique for realizing the SPA and SFA. Finally, applications of the SP- or SF-based intelligent control technique for optimization of cultivating and storage processes are provided, aiming at qualitative improvement of plants and fruits.*

***Keywords.*** *SPA, SFA, Sensors, Plant responses, Fruit responses, Measurement, Identification, Optimization, Environmental control, Speaking plant, Speaking fruit.*